# ESTIMATING BIOMASS OF *MELALEUCA CAJUPUTI* FOREST ECOSYSTEMS BASED ON MULTI-SOURCE SATELLITE DATA IN MEKONG DELTA, VIETNAM

LUONG, N. V.[1*] – THE ANH, L.[2]

[1]*Vietnam National Space Center, Vietnam Academy of Science & Technology, 18 Hoang Quoc Viet str., Nghia Do ward, Hanoi 100000, Vietnam*

[2]*Central Institute for Natural Resources and Environmental Studies, Vietnam National University, Hanoi 100000, Vietnam*

[*]*Corresponding author*
*e-mail: nvluong@vnsc.org.vn; phone: +84-243-756-2985; fax: +84-243-791-4622*

(Received 9th Sep 2025; accepted 3rd Dec 2025)

**Abstract.** Melaleuca forests in the U Minh Thuong ASEAN Heritage Park, the Mekong Delta of Vietnam involve a distinctive ecosystem that contributes significantly to biodiversity conservation and the provision of essential ecosystem services. Despite their importance, methods for accurately estimating carbon stocks in these forests remain insufficiently studied. This study utilizes both RADAR and optical data from ALOS-2, Sentinel-1, Landsat 8, and Sentinel-2 satellites to model and map the spatial distribution of aboveground biomass (AGB) in *Melaleuca* forests within U Minh Thuong National Park, a tropical forest site in the Mekong Delta of Vietnam. Various models were constructed using the backscatter values and Gray Level Co-occurrence Matrix (GLCM) calculated from RADAR data and normalized difference vegetation index (NDVI) from optical data, and field estimated AGB. For modelling, k-fold cross-validation approach was used. The study also found that the model integrating ALOS-2 PALSAR-2 HV data, GLCM textures, and Sentinel-2 NDVI, showed the best results ($R^2 = 0.84$, RMSE = 9.59 Mg $ha^{-1}$). The research underscores the significance of remote sensing data in supporting conservation efforts and sustainable forest management practices in tropical ecosystems. The study contributes to advancing biomass estimation methodologies and emphasizes the importance of multi-sensor satellite data integration for accurate and reliable forest biomass mapping, particularly in ecologically sensitive regions like the U Minh Thuong National Park.
**Keywords:** *aboveground biomass, U Minh Thuong National Park, Melaleuca forest, heritage park, ALOS-2 PALSAR-2, Sentinel 1&2, Landsat 8 OLI*

## Introduction

*Melaleuca cajuputi* forests form a unique ecosystem in the coastal wetlands in tropical and subtropical zones (Tran et al., 2013). They are primarily located in Australia, New Guinea, the southern parts of United States, the Caribbean, Malaysia, Thailand, Cambodia, and Vietnam (Bartolo, 2005; Tran et al., 2013). In Vietnam, they are concentrated in the Mekong Delta. These forests provide vital ecological and socio-economic services, supporting biodiversity by offering habitats for various species and supplying timber, charcoal, fuelwood, oil, and honey. The carbon sequestration of these forests plays a critical role in mitigating climate change (Bartolo et al., 2005; Tran et al., 2005; RSIS, 2015; Xiang et al., 2025). Therefore, precise biomass estimation is essential for evaluating carbon stock levels (Raihan et al., 2021; Huang et al., 2022).

Traditional aboveground biomass (AGB) assessment methods rely on extensive field inventories, which are labour-intensive and impractical in inaccessible areas, limiting their use to small regions. In contrast, geospatial technology provides a more efficient and cost-effective approach for AGB mapping, monitoring, and modelling in large regions


http://www.aloki.hu ● ISSN 1589 1623 (Print) ● ISSN 1785 0037 (Online)
DOI: http://dx.doi.org/10.15666/aeer/2401_14531466

(Lu, 2006; Kushwaha et al., 2014; Manna et al., 2014; Kalita et al., 2022). However, field data continue to play a crucial role in the training and validation of remote sensing (RS)-based AGB estimates. An extensive array of RS datasets, including optical multispectral and hyperspectral imagery as well as active sensor data such as light detection and ranging (LiDAR) and synthetic aperture radar (SAR), are now readily accessible and increasingly utilized for AGB estimation and monitoring. These datasets offer varying spatial, spectral, and temporal resolutions, enabling researchers to capture vegetation structure, canopy properties, and biomass-related parameters with improved accuracy and scale (Li et al., 2018; Nandy et al., 2019; Singh et al., 2023; Luong et al., 2025).

Recent technological advancements and the growing availability of data have allowed researchers to combine various satellite datasets, enhancing the precision of forest biomass estimation (Luong et al., 2019; Dang et al., 2019; Opelele et al., 2021; Bhandari and Nandy, 2024). However, challenges remain, particularly in large, complex environments such as tropical forests. Additionally, the lack of equations for converting biomass from the basic parameters of individual forest trees has led to discrepancies in research findings, undermining their scientific robustness (Baskent et al., 1995; Xiao et al., 2019; Huang et al., 2022). SAR remote sensing is ideally suited for tropical regions, as it penetrates cloud cover and dense vegetation. Its all-weather, day-and-night capability enables reliable estimation of forest structure as well as biomass (Mougin et al., 1999; Hamdan et al., 2015; Luong et al., 2016; Omar et al., 2017; Tuong et al., 2019; Golshani et al., 2019; Luong et al., 2024).

Despite early efforts to use remote sensing data for mapping Melaleuca forests (Williams, 1984; Bartolo, 2005; Ibrahim et al., 2012), there has been a lack of attention towards estimating Melaleuca forest biomass using remote sensing, particularly in Vietnam (Bartolo, 2005). Therefore, this study aims to develop models, using various combinations of ALOS-2 PALSAR-2, Sentinel-1, Sentinel-2 and Landsat 8 OLI, for AGB estimation and to map the AGB in Melaleuca forests in U Minh Thuong National Park, Mekong Delta in Vietnam. This will support conservation efforts and promote sustainable forest management within this unique tropical ecosystem.

## Method and material

### *Study area*

The U Minh Thuong National Park is located to the westward of the Ca Mau peninsula in An Giang Province, Mekong Delta in Vietnam. It is approximately 365 km southwest of Ho Chi Minh City. The park covers a total area of 8,038 ha (Tran, 2013). The study area (9°31′16″ to 9°39′45″ N latitude and 105°03′06″ to 105°07′59″ E longitude) is geographically located in An Minh Bac and Minh Thuan communes of U Minh Thuong District, An Giang Province (*Figure 1*). Importantly, the park is designated as one of the top three sites prioritized for wetland conservation in Vietnam's Mekong Delta region (RSIS, 2015).

U Minh Thuong National Park harbours a distinctive ecosystem characterized by Melaleuca forests on swam and peat. The dominant arboreal species, Melaleuca (*Melaleuca cajuputi*), forms the predominant constituent of the forest canopy. However, alongside Melaleuca, several other tree species such as *Alstonia spathulata, Ilex cymosa, Euodia lepta, Syzygium cumini, Elaeocarpus hygrophylus*, as well as various grasses and shrubs including *Phragmites vallatoria, Eleocharis dulcis, Stenochlaena palustris* and *Nephrolepis falcate*, are also found in the forest. The park supports numerous rare and


http://www.aloki.hu ● ISSN 1589 1623 (Print) ● ISSN 1785 0037 (Online)
DOI: http://dx.doi.org/10.15666/aeer/2401_14531466

threatened species. The rare plant species recorded include *Elaeocarpus hygrophilus* Kurz., *Hydnophytum formicarum* Jack., *Eulophia graminea* Lindl., *Pachystoma pubescens* Blume., and *Spiranthes sinensis* (Pers.) Ames. The rare animal species recorded include *Lutra sumatrana*; *Prionailurus viverrinus*, *Manis javanica*, *Pteropus lylei*, *Leptoptilos javanicus*, *Mycteria leucocephala*, *Pelecanus philippensis*, *Cuora amboinensis*, *Heosemys annandalii*, and *Malayemys subtrijuga*, and its Melaleuca forest on swamp peatland represents a distinctive and endemic ecosystem of the lower Mekong Delta in Vietnam (Tran, 2013; Truong et al., 2024).

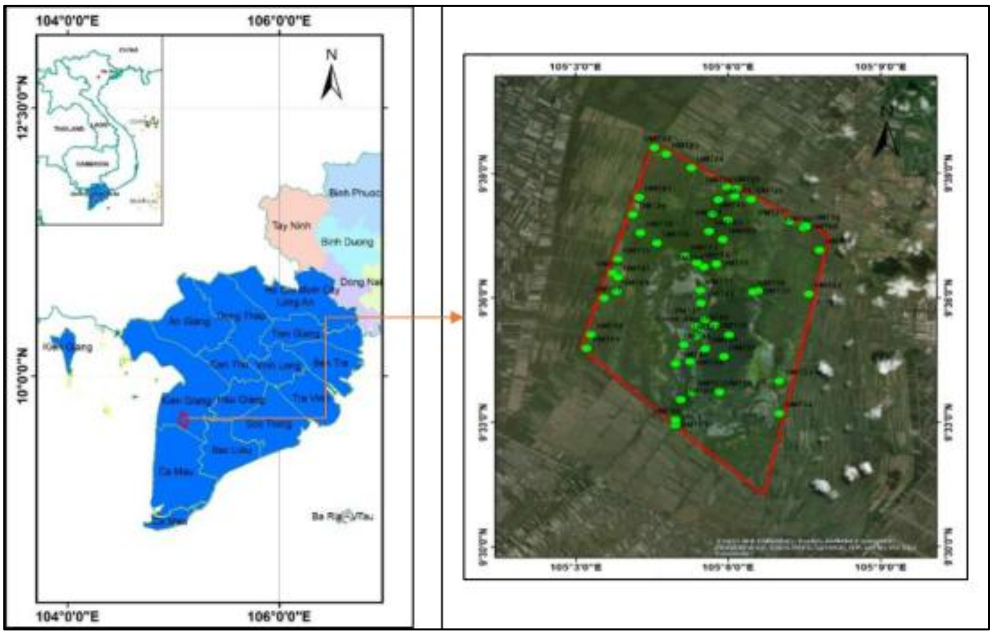


***Figure 1.*** *Study area map with sample plot locations represented by green points*

The park, recognized in August 2013 as the first ASEAN Heritage Park designated on peatland in Vietnam, plays a crucial role in conserving its extensive peat layers and acting as a natural hydrological buffer by regulating groundwater and distributing surface water to nearby areas, essential for sustaining local livelihoods. The park also holds significant spiritual, historical, archaeological, educational, and scientific value (Tsitsi, 2016).

Some field survey photos are shown in *Figure 2*.

## *Methodology*

### *Field data collection and biomass calculation*

Sample plots were established across the study area during a field survey carried out in October 2018. The size of each sample plot is 500 m² (20 m × 25 m). A total of 54 sample plots were established and evenly distributed across the study area. The location and distribution of sample plots are shown in *Figure 1*. In each sample plots, the diameter at 1.3 m position, and height of all trees having a diameter greater than 5 cm were measured using laser measured by diameter laser meters (Criterion RD1000) and lasers measuring height (Trupulse 360B). The device was manufactured by Laser Technology Inc. (LTI), Origin: USA. The geographic coordinates at the centre of all the sample plots


http://www.aloki.hu ● ISSN 1589 1623 (Print) ● ISSN 1785 0037 (Online)
DOI: http://dx.doi.org/10.15666/aeer/2401_14531466

were recorded using Garmin GPSMAP 87S GPS instrument (Garmin Ltd., Origin: USA). AGB was calculated using *Equation 1* (Dan et al., 2014).

$$AGB = 0.3188 \times {D_{1.3}}^{2.1672} \quad \text{(Eq.1)}$$

where, $AGB$ is the aboveground biomass of a tree (kg); $D_{1.3}$ is the diameter at 1.3 m position.


***Figure 2.** Field survey photos of the study area*

The calculated fresh biomass was then converted to dry biomass by multiplying with the conversion factor of 0.5, following Hồng et al. (2015). A summary of the field survey results is presented in *Table 1*.

***Table 1.** Summary of the surveyed variables in the research site*

| No. | Forest variable | Minimum | Maximum | Median | Standard deviation |
|---|---|---|---|---|---|
| 1 | Diameter (cm) | 5.61 | 23.16 | 8.44 | 2.74 |
| 2 | Height (m) | 3.66 | 12.16 | 5.14 | 2.05 |
| 3 | Density (tree $ha^{-1}$) | 160 | 6260 | 550 | 1,550 |
| 4 | Biomass (Mg $ha^{-1}$) | 2.20 | 115.30 | 10.12 | 27.21 |

*Satellite data*

The satellite data used in the study was selected based upon the accessibility, present and future availability, and their applicability in biomass studies. Synthetic Aperture Radar (SAR) data acquired from ALOS-2 PALSAR-2 (L-band) and Sentinel-1 (C-band)


http://www.aloki.hu ● ISSN 1589 1623 (Print) ● ISSN 1785 0037 (Online)
DOI: http://dx.doi.org/10.15666/aeer/2401_14531466

were employed in the study. ALOS-2 PALSAR-2 level 2.1 data with 10 m resolution including HH and HV polarizations and Sentinel-1 data with 10 m resolution and VH and VV polarizations were used in the present study. To calculate the NDVI, optical satellite data from the Landsat 8 OLI and Sentinel-2 MSI were employed. The description of the satellite image used in this study is provided in *Table 2*.

***Table 2.*** *Satellite imagery used in this study*

| No. | Satellite Sensors | Observation date (day, month, year) | Pixel resolution (m) | Polarizations/Band (Indices used) |
|---|---|---|---|---|
| 1 | ALOS-2 PALSAR-2 | 30-08-2018 | 10 | HH, HV |
| 2 | Sentinel-1 | 02-11-2018 | 10 | VH, VV |
| 3 | Landsat 8 OLI | 31-10-2018 | 30, 15 | Band 4, Band 5, Band 8 (NDVI) |
| 4 | Sentinel-2 MSI | 02-11-2018 | 10 | Band 4, Band 8 (NDVI) |

*Satellite data processing and variable extraction*

The RADAR images were radiometrically corrected, filter to remove noise, and terrain corrected.

Digital number (DN) values from ALOS-2 PALSAR-2 Level 2.1 imagery were converted into sigma naught backscattering intensities ($\sigma^0$) in *Equation 2* (JAXA, 2017).

$$\sigma^o = 10 \times log_{10}(DN^2) + CF \qquad \text{(Eq.2)}$$

where, $\sigma^o$ is backscattering intensity (dB), DN is digital number values, and CF is the calibration factor (constant, set at -83 (JAXA, 2017)).

Similarly, the DN values from Sentinel-1 data were converted to the backscatter values using *Equation 3* (ESA, 2019).

$$\sigma^o = DN^2/\, {A_\sigma}^2 \qquad \text{(Eq.3)}$$

where, $\sigma^o$ is backscattering intensity (dB), DN is digital number values and ${A_\sigma}^2$ is the reference area of the scattering surface.

Image texture was analyzed using the Gray Level Co-occurrence Matrix (GLCM) technique applied to different polarizations of ALOS-2 PALSAR-2 data. The extracted texture variables included contrast, correlation, dissimilarity, entropy, homogeneity, mean, second angular moment and variance (Haralick et al., 1973).

Top-of-atmosphere (TOA) reflectance data from Landsat 8 OLI and Sentinel-2 were acquired and pre-processed, focusing on cloud-free observations over the study area. The NDVI was then calculated for both sensors using *Equation 4* (Rouse et al., 1974).

$$\text{NDVI} = \frac{\text{NIR}-\text{RED}}{\text{NIR}+\text{RED}} \qquad \text{(Eq.4)}$$

where NIR is the near-infrared spectral band and RED is the red spectral band.

The sample plot positions were used to extract the independent variables for AGB model development.


http://www.aloki.hu ● ISSN 1589 1623 (Print) ● ISSN 1785 0037 (Online)
DOI: http://dx.doi.org/10.15666/aeer/2401_14531466

*Cross-validation approach*

In this study, the model training was conducted using a k-fold cross-validation approach. The k-fold approach works by dividing the training set into k subsets of equal size without a common element. In each run, one of the 'k' subsets is taken out as a validation set and the model is built using the remaining 'k-1' subsets. The final model is determined based on the average of the training and validation errors. In this study, the training data was split into 4 subsets (k = 4).

*Model validation and accuracy assessment*

A set of 25% of the sample plots was selected randomly for validation purposes. This dataset is independent of the dataset used to run the model. Model accuracy was assessed using the coefficient of determination ($R^2$; *Equation 5*) and the root mean square error (RMSE; *Equation 6*) as performance evaluation metrics.

$$R^2 = 1 - \frac{\text{Explained Sum of Squares}}{\text{Total Sum of Squares}} \qquad \text{(Eq.5)}$$

$$\text{RMSE} = \sqrt{\frac{1}{n}\sum_{j=1}^{n}(\text{Predicted AGB value} - \text{Observed AGB value})^2} \qquad \text{(Eq.6)}$$

where the predicted AGB value is the AGB value obtained from the model; Observed AGB biomass value is the AGB value from the inventory data, and n is the number of sample plots used.

## Result

### *AGB models using parameters from a single satellite*

Using the variables extracted from single satellite data, various AGB models were constructed using the k-fold cross-validation technique. A total of 20 models, using the single satellite variables were constructed, and their cross-validation $R^2$ and RMSE were calculated (*Table 3*).

*Table 3* shows that some of these models (model 4, model 18, and model 20) showed high $R^2$/RMSE values (0.83/9.88, 0.82/10.17, and 0.82/10.17).

### *Biomass models using a combination of parameters from different satellites*

AGB models were developed by integrating variables derived from ALOS-2 PALSAR-2, Landsat 8 OLI, and Sentinel-2 datasets. A total of 10 combined models were constructed (*Table 4*). The best model ($R^2$ = 0.84, RMSE = 9.59) was achieved using a combination of variables, including HV polarization backscatter and GLCM-derived texture features from ALOS-2 PALSAR-2, along with NDVI from Sentinel-2 imagery.

### *Biomass mapping*

The model 28 consisted of ALOS-2 PALSAR-2 HV polarization, GLCM from HV polarization, and Sentinel-2 NDVI as independent variables. On validation, the model was found to have an $R^2$ of 0.84, RMSE = 9.59 Mg $ha^{-1}$ (*Figure 3*). Model 28, which


http://www.aloki.hu ● ISSN 1589 1623 (Print) ● ISSN 1785 0037 (Online)
DOI: http://dx.doi.org/10.15666/aeer/2401_14531466

demonstrated the highest predictive performance, was applied to map the spatial distribution of AGB in the study area (*Figure 4*).

Based upon the forest AGB map, it was found that of the total area of 8,038.26 ha, 16.01% (1,286.92 ha) is rich forest biomass area with forest AGB ranging from 100 Mg $ha^{-1}$ and above. Whereas 39.75% (3,195.11 ha) of the area is medium biomass forest with AGB ranging between 50 to 100 Mg $ha^{-1}$, and 32.63% (2,623.07 ha) of the area was low biomass forest with AGB lower than 50 Mg $ha^{-1}$. and 11.61% (933.16 ha) of non-forest.

***Table 3.*** *Summary of the AGB estimation models*

| No. | Variable used | AGB model | $R^2$ | RMSE |
|---|---|---|---|---|
| **ALOS-2 PALSAR-2 satellite (L-band)** | | | | |
| Model 1 | HH | AGB = 92.54 + 8.009*HH | 0.34 | 19.47 |
| Model 2 | HH | AGB = 19.14 + 87.74*HH + 59.55*HH$^2$ | 0.50 | 16.95 |
| Model 3 | HV | AGB = 199.13 + 11.97*HV | 0.68 | 13.56 |
| Model 4 | HV | AGB = 19.14 + 123.67*HV + 62.76*HV$^2$ | 0.83 | 9.88 |
| Model 5 | (HH+HV)/2 | AGB = 161.27 + 11.74*(HH+HV)/2 | 0.59 | 15.34 |
| Model 6 | (HH+HV)/2 | AGB = 19.15 + 114.67*(HH+HV)/2 + 66.73*[(HH+HV)/2]$^2$ | 0.79 | 10.98 |
| Model 7 | (HH×HH/HV) + HV | AGB = 140.07 + 5.83*(HV+HH*HH/HV) | 0.51 | 16.78 |
| Model 8 | (HH×HH/HV) + HV | AGB = 19.14 + 106.57*(HV+HH*HH/HV) + 69.63*(HV+HH*HH/HV)$^2$ | 0.72 | 12.68 |
| Model 9 | HH, HV | AGB = 198.14 + 0.57*HH + 11.55*HV | 0.68 | 13.56 |
| Model 10 | Grey-level co-occurrence matrix (GLCM) | AGB = -143.21 – 5.17*Contrast + 1.68*Correlation + 109.61*Dissimilarity – 71.14*Entropy – 517.48*Homogeneity + 0.94*Mean – 794.70*SecondMoment – 2.13*Variance | 0.24 | 20.89 |
| Model 11 | GLCM and HH | AGB = -409.99 + 11.50*HH - 1.54*Contrast + 27.32*Correlation + 60.72*Dissimilarity + 148.43*Entropy + 333.65*Homogeneity – 6.45*Mean + 2132.99*SecondMoment – 2.43*Variance | 0.65 | 14.18 |
| Model 12 | GLCM and HV | AGB = 109.07 + 12.27*HV – 2.81*Contrast + 4.27*Correlation + 40.76*Dissimilarity – 41.54*Entropy + 228.71*Homogeneity + 1.64*Mean – 192.38*SecondMoment + 2.78*Variance | 0.79 | 10.98 |
| **Sentinel-1 satellite (C-band)** | | | | |
| Model 13 | VH | AGB = 145.06 + 8.08*VH | 0.36 | 19.17 |
| Model 14 | VH | AGB = 19.14 + 90.38*VH+ 51.11*(VH)$^2$ | 0.48 | 17.28 |
| Model 15 | VV | AGB = 88.58 + 5.95*VV | 0.24 | 20.89 |
| Model 16 | VV | AGB = 19.14 + 73.74*VV+ 46.85*(VV)$^2$ | 0.34 | 19.47 |
| | | AGB = 12.58 + 12.41*VH – 4.28*VV | 0.39 | 18.72 |
| **Landsat 8 OLI satellite** | | | | |
| Model 17 | Landsat 8 Normalized difference vegetation index (NDVI_LS8) | AGB = -42.45 + 130.23*NDVI_LS8 | 0.61 | 14.97 |
| Model 18 | NDVI_LS8 | AGB = 19.14 + 117.14*NDVI_LS8 + 67.41*(NDVI_LS8)$^2$ | 0.82 | 10.17 |
| **Sentinel-2 satellite** | | | | |
| Model 19 | Sentinel 2 Normalized difference vegetation index (NDVI_S2) | AGB = - 45.68 + 140.58*NDVI_S2 | 0.68 | 13.56 |
| Model 20 | NDVI_S2 | AGB = 19.15 + 123.42*NDVI_S2 + 56.42*(NDVI_S2)$^2$ | 0.82 | 10.17 |


http://www.aloki.hu ● ISSN 1589 1623 (Print) ● ISSN 1785 0037 (Online)
DOI: http://dx.doi.org/10.15666/aeer/2401_14531466

***Table 4.*** *Summary of the AGB estimation models developed using integrated optical and radar satellite data*

| No. | Variable used | AGB model | $R^2$ | RMSE |
|---|---|---|---|---|
| **ALOS – 2 PALSAR -2 and Landsat 8 OLI satellites** | | | | |
| Model 21 | GLCM and NDVI_LS8 | AGB = 89.82 - 2.25*Contrast + 4.53*Correlation + 39.90*Dissimilarity - 77.74*Entropy + 201.60*Homogeneity + 1.08*Mean - 1460.66*SeconMoment - 0.55*Variance + 122.30*NDVI_LS8 | 0.65 | 14.18 |
| Model 22 | HH, GLCM and NDVI_LS8, | AGB = - 164.02 + 7.35*HH + 78.50*NDVI_LS8 - 0.97*Contrast + 19.89*Correlation + 33.63*Dissimilarity + 64.90*Entropy + 197.27*Homogeneity - 3.68*Mean + 648.33*SeconMoment - 1.31*Variance | 0.76 | 11.74 |
| Model 23 | HV, GLCM and NDVI_LS8 | AGB = 137.04 + 9.63*HV + 43.22*NDVI_LS8 - 2.293*Contrast + 4.72*Correlation + 30.96*Dissimilarity - 50.25*Entropy + 179.33*Homogeneity + 1.54*Mean - 557.59*SecondMoment + 2.28*Variance | 0.82 | 10.17 |
| Model 24 | HH, NDVI_LS8 | AGB = 6.31 + 4.19*HH + 108.31*NDVI_LS8 | 0.69 | 13.34 |
| Model 25 | HV, NDVI_LS8 | AGB = 106.77 + 7.91*HV + 66.22*NDVI_LS8 | 0.76 | 11.74 |
| **ALOS – 2 PALSAR -2 and Sentinel -2 satellites** | | | | |
| Model 26 | NDVI_S2, GLCM | AGB = - 1.92 + 132.08*NDVI_S2 - 1.53*Contrast - 6.84*Correlation + 27.23*Dissimilarity - 38.00*Entropy + 170.15*Homogeneity + 0.56*Mean - 1071.15*SeconMoment + 0.13*Variance | 0.72 | 12.8 |
| Model 27 | HH, GLCM and NDVI_ S2 | AGB = - 191.59 + 6.37*HH + 92.82*NDVI_S2 - 0.60*Contrast + 9.88*Correlation + 24.65*Dissimilarity + 73.72*Entropy + 171.60*Homogeneity - 3.41*Mean + 632.09*SeconMoment - 0.70*Variance | 0.80 | 10.72 |
| Model 28 | HV, GLCM and NDVI_ S2 | AGB = 94.90 + 8.35*HV + 61.99*NDVI_S2 - 1.8637*Contrast - 0.55*Correlation + 24.06*Dissimilarity - 35.43*Entropy + 157.81*Homogeneity + 1.24*Mean - 514.31*SeconMoment + 2.27*Variance | 0.84 | 9.59 |
| Model 29 | HH, NDVI_ S2 | AGB = -5.09 + 3.40*HH + 120.28*NDVI_S2 | 0.73 | 12.45 |
| Model 30 | HV, NDVI_ S2 | AGB = 86.74 + 6.98*HV + 81.17*NDVI_S2 | 0.79 | 10.98 |

| No. | Field-measured AGB (Mg $ha^{-1}$) | Predicted AGB (Mg $ha^{-1}$) |
|---|---|---|
| 1 | 27.18 | 30.46 |
| 2 | 15.09 | 28.93 |
| 3 | 10.72 | 28.32 |
| 4 | 65.21 | 46.29 |
| 5 | 31.46 | 4.93 |
| 6 | 36.52 | 5.53 |
| 7 | 41.01 | 9.15 |
| 8 | 11.21 | 47.39 |
| 9 | 230.60 | 217.93 |
| 10 | 39.49 | 17.50 |
| 11 | 21.90 | 33.78 |
| 12 | 5.88 | 40.74 |
| 13 | 173.94 | 119.09 |
| 14 | 126.80 | 122.22 |

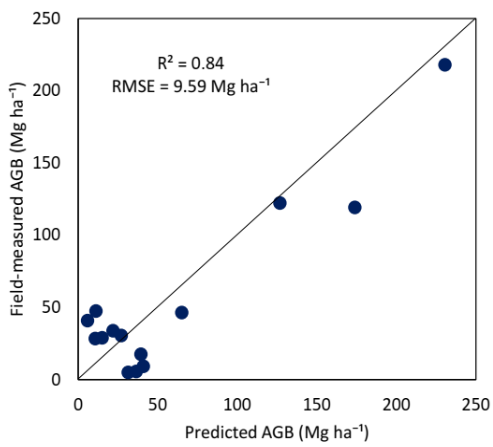


***Figure 3.*** *The validation results are shown in the 1:1 cross-plot comparing predicted and field-measured AGB*

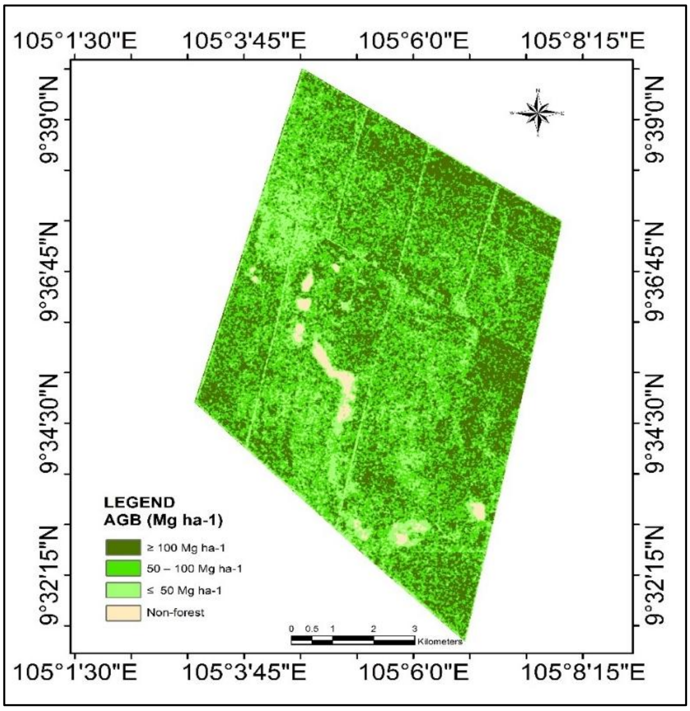


***Figure 4.*** *Spatial distribution of forest AGB in U Minh Thuong National Park*

## Discussions

In this study, satellite data from ALOS-2 PALSAR-2, Sentinel-1, Sentinel-2 and Landsat 8 OLI satellites were utilized to assess the applicability of variables extracted from these datasets, such as backscattering intensity, GLCM-based textures, and NDVI for estimating Melaleuca forest AGB. The variables extracted from these satellite datasets were found to be highly correlated with the field-measured AGB in the Melaleuca forest, except for data from the Sentinel-1 satellite, because this limitation also applies to the C-band SAR in moist tropical forests due to poor canopy penetration. Despite this exception, our results surpass those of previous studies conducted by Omar et al. (2020), Khan et al. (2020) and Stratoulias et al. (2022) when using only one type of optical satellite imagery.

Our analysis reveals that each satellite, including ALOS-2 PALSAR-2, Landsat 8 OLI, and Sentinel-2, has the potential to estimate the forest AGB with high accuracy. Each of these datasets showed high $R^2$ for at least one of the extracted variables while developing the forest AGB models. The performances of these simple models can also be attributed to the fact that the AGB of the Melaleuca forest in the study area is not extremely high. However, the combination of multiple satellite data sensors enhanced the performance of the biomass model. This integration has reduced the problem of data saturation, and has improved the estimation of forest AGB (Zhao et al., 2016; Khan et al., 2020; Ahmad et al., 2021).

When considering only the variables extracted from individual satellite datasets as the independent variables for constructing the biomass models, Model 4, utilizing the backscatter values from HV polarization of ALOS-2 PALSAR-2 data, Model 18 utilizing the NDVI calculated from Landsat 8 OLI data, and Model 20 utilizing the NDVI calculated from Sentinel-2 data exhibited noteworthy performance, explaining 84%, 82%, and 82% variability in the Melaleuca forest AGB, respectively.


http://www.aloki.hu ● ISSN 1589 1623 (Print) ● ISSN 1785 0037 (Online)
DOI: http://dx.doi.org/10.15666/aeer/2401_14531466

Models developed using the combination of parameters from different satellites yielded high $R^2$ values. Model 23 incorporating ALOS-2 PALSAR-2 HV data, GLCM textures, and Landsat 8 NDVI ($R^2 = 0.82$; RMSE = 10.17 Mg $ha^{-1}$), Model 27 integrating ALOS-2 PALSAR-2 HH data, textures, and Sentinel-2 NDVI ($R^2 = 0.80$; RMSE = 10.72 Mg $ha^{-1}$), and Model 28 combining ALOS-2 PALSAR-2 HV data, textures, and Sentinel-2 NDVI ($R^2 = 0.84$; RMSE = 9.59 Mg $ha^{-1}$) exhibited high accuracies.

Our results surpass those of recent studies, such as those by Vafaei et al. (2018), Zhu et al. (2020), and López et al. (2020), due to the unique characteristics of our study area, characterized by flat topography, sparse forest tree density, predominantly small to medium-sized trees, and relatively low biomass reserves. Consistent with prior research by Lucas et al. (2010) and Luong et al. (2016, 2019), we also found that backscattering intensity at HV polarization exhibits greater sensitivity compared to HH polarization. This can be attributed to the fact that the dominant scattering mechanisms in forests, such as volume scattering, are more effectively captured by HV polarization due to its ability to penetrate vegetation canopies and interact with vertical components of vegetation, such as stems and branches.

## Conclusions

This study utilized ALOS-2 PALSAR-2, Sentinel-1, Sentinel-2, and Landsat 8 OLI satellites to estimate the spatial distribution of AGB in the Melaleuca forest in the Mekong Delta region of Vietnam. In total, 30 models using various variables from individual satellite datasets and combinations of these datasets were constructed using a k-fold cross-validation approach. The results reflected that in the present ecological settings, where Melaleuca forest with moderate forest AGB grows on peat soils, the capacity of RADAR (ALOS-2 PALSAR-2) and optical (Landsat 8, Sentinel-2) datasets for AGB estimation was comparable. This study reiterates the fact that the sensitivity of backscattering intensity at HV is more than that of backscattering intensity at HH. The study also highlighted the importance of the synergistic use of RADAR and optical data for forest AGB estimation. The results of this study offer a scientific foundation to support decision-making related to conservation, sustainable development strategies, and potential engagement in carbon emission trading mechanisms for U Minh Thuong National Park, located in the Mekong Delta region of Vietnam.

**Acknowledgements.** The authors are grateful to project No. VAST01.03/23-24 from the Vietnam Academy of Science and Technology (VAST) for supporting this research. The authors acknowledge the U.S. Geological Survey for providing Landsat data and express their gratitude to JAXA for ALOS-2 PALSAR-2 (PI Number; ER3A2N520) data and the European Space Agency for access to Sentinel-1 and Sentinel-2 data.

## REFERENCES

[1] Ahmad, A., Gilani, H., Ahmad, S. R. (2021): Forest aboveground biomass estimation and mapping through high-resolution optical satellite imagery: A literature review. – Forests 12(7): 914. https://doi.org/10.3390/f12070914.

[2] Bartolo, R. E. (2005): Remote sensing of Melaleuca biomass on tropical floodplains. – Doctoral dissertation, Charles Darwin University.

[3] Baskent, E. Z., Jordan, G. A. (1995): Characterizing spatial structure of forest landscapes. – Canadian Journal of Forest Research 25(11): 1830-1849. https://doi.org/10.1139/x95-198.
[4] Bhandari, S. K., Nandy, S. (2024): Forest aboveground biomass prediction by integrating terrestrial laser scanning data, Landsat 8 OLI-derived forest canopy density and spectral indices. – Journal of the Indian Society of Remote Sensing 52(4): 813-824. https://doi.org/10.1007/s12524-023-01687-z.
[5] Dan, T. H., Lê Hoàng Tất, B. T. T. (2014): Đánh giá lượng cacbon tích lũy của sinh khối rừng tràm trên nền đất sét tại Vườn Quốc gia U Minh Thượng. – Tạp chí Khoa học Trường Đại học Cần Thơ, 125-135.
[6] Dang, A. T. N., Nandy, S., Srinet, R., Luong, N. V., Ghosh, S., Kumar, A. S. (2019): Forest aboveground biomass estimation using machine learning regression algorithm in Yok Don National Park, Vietnam. – Ecological Informatics 50: 24-32. https://doi.org/10.1016/j.ecoinf.2018.12.010.
[7] ESA (2019): You've lost your orbit, captain! – The European Space Agency. https://esa.int/web/sentinel/technical-guides/Sentinel-1-sar.
[8] Golshani, P., Maghsoudi, Y., Sohrabi, H. (2019): Relating ALOS-2 PALSAR-2 Parameters to Biomass and Structure of Temperate Broadleaf Hyrcanian Forests. – Journal of the Indian Society of Remote Sensing 47(5): 749-761. https://doi.org/10.1007/s12524-019-00948-0.
[9] Hamdan, O., Hasmadi, I. M., Aziz, H. K., Norizah, K., Zulhaidi, M. H. (2015): L-band saturation level for aboveground biomass of dipterocarp forests in peninsular Malaysia. – Journal of Tropical Forest Science 27(3): 388-399.
[10] Haralick, R. M., Shanmugam, K., Dinstein, I. H. (1973): Textural features for image classification. – IEEE Transactions on Systems, Man, and Cybernetics 6: 610-621. doi: 10.1109/TSMC.1973.4309314.
[11] Hồng, T. T. K., và Lê Thị, Q. T. X., Hằng, N. (2015): Sinh khối rừng tràm Vườn Quốc gia U Minh Thượng, tỉnh Kiên Giang. – Tạp chí Khoa học Trường Đại học Cần Thơ 37: 63-68. https://doi.org/10.1155/2014/715796.
[12] Huang, C. Q., Gong, W. S., Pang, Y. (2022): Remote Sensing and Forest Carbon Monitoring--a Review of Recent Progress, Challenges and Opportunities. – Journal of Geodesy & Geoinformation Science 5(2): 124-147. DOI: 10.11947/j.JGGS.2022.0212.
[13] Ibrahim, I. F., Balasundram, S. K., Nur-Ashikin, P. A., Sood, A. M., Makhdzir, M., Saberioon, M. M. (2012): The spatial distribution of *Apis dorsata* host plants using an integrated geographical information system-remote sensing approach. – American Journal of Agricultural and Biological Sciences 7(4): 396-406. https://doi.org/10.3844/ajabssp.2012.396.406.
[14] JAXA (2017): Calibration Result of ALOS-2/PALSAR-2 JAXA Standard Products. – https://www.eorc.jaxa.jp/ALOS-2/en/calval/calval_index.htm.
[15] Kalita, R. M., Nandy, S., Srinet, R., Nath, A. J., Das, A. K. (2022): Mapping the spatial distribution of aboveground biomass of tea agroforestry systems using random forest algorithm in Barak valley, Northeast India. – Agroforestry Systems 96(8): 1175-1188. https://doi.org/10.1007/s10457-022-00776-1.
[16] Khan, K., Iqbal, J., Ali, A., Khan, S. N. (2020): Assessment of Sentinel-2-derived vegetation indices for the estimation of above-ground biomass/carbon stock, temporal deforestation and carbon emissions estimation in the moist temperate forests of Pakistan. – Applied Ecology & Environmental Research 18(1): 783-815. DOI: http://dx.doi.org/10.15666/aeer/1801_783815.
[17] Kushwaha, S. P. S., Nandy, S., Gupta, M. (2014): Growing stock and woody biomass assessment in Asola-Bhatti Wildlife Sanctuary, Delhi, India. – Environmental Monitoring and Assessment 186(9): 5911-5920. https://doi.org/10.1007/s10661-014-3828-0.
[18] Li, X., Du, H., Mao, F., Zhou, G., Chen, L., Xing, L., Fan, W., Xu, X., Liu, Y., Cui, L., Zhu, D., Li, Y. (2018): Estimating bamboo forest aboveground biomass using EnKF-


http://www.aloki.hu ● ISSN 1589 1623 (Print) ● ISSN 1785 0037 (Online)
DOI: http://dx.doi.org/10.15666/aeer/2401_14531466

assimilated MODIS LAI spatiotemporal data and machine learning algorithms. – Agricultural and Forest Meteorology (256-257): 445-457. https://doi.org/10.1016/j.agrformet.2018.04.002.

[19] López-Serrano, P. M., Cárdenas Domínguez, J. L., Corral-Rivas, J. J., Jiménez, E., López-Sánchez, C. A., Vega-Nieva, D. J. (2020): Modeling of Aboveground Biomass with Landsat 8 OLI and Machine Learning in Temperate Forests. – Forests 11(1): 11. https://doi.org/10.3390/f11010011.

[20] Lu, D. (2006): The potential and challenge of remote sensing-based biomass estimation. – International Journal of Remote Sensing 27(7): 1297-1328. https://doi.org/10.1080/01431160500486732.

[21] Lucas, R., Armston, J., Fairfax, R., Fensham, R., Accad, A., Carreiras, J., Kelley, J., Bunting, P., Clewley, D., Bray, S., Metcalfe, D., Dwyer, J., Bowen, M., Eyre, T., Laidlaw, M., Shimada, M. (2010): An evaluation of the ALOS PALSAR L-band backscatter—Above ground biomass relationship Queensland, Australia: Impacts of surface moisture condition and vegetation structure. – IEEE Journal of selected topics in applied earth observations and remote sensing 3(4): 576-593. doi:10.1109/JSTARS.2010.2086436.

[22] Luong, N. V., Tateishi, R., Kondoh, A., Sharma, R., Thanh Nguyen, H., Trong To, T., Ho Tong Minh, D. (2016): Mapping tropical forest biomass by combining ALOS-2, Landsat 8, and field plots data. – Land 5(4): 31. https://doi.org/10.3390/land5040031.

[23] Luong, N. V., Tu, T. T., Khoi, A. L., Hong, X. T., Hoan, T. N., Thuy, T. L. H. (2019): Biomass Estimation and Mapping of Can Gio Mangrove Biosphere Reserve in South of Viet Nam Using Alos-2 Palsar-2 Data. – Applied Ecology and Environmental Research 17(1): 15-31. DOI: http://dx.doi.org/10.15666/aeer/1701_015031.

[24] Lương, N. V., Khắc, Đ. V., Chiến, N. Q., Vân Anh, N. T., Sơn, N. T. T. (2024): Ứng dụng công nghệ viễn thám và GIS ước tính sinh khối rừng thông ba lá (*Pinus kesiya* royle ex gordon) khu vực hồ Tuyền Lâm, thành phố Đà Lạt, tỉnh Lâm Đồng. – Tạp chí Khoa học Đo đạc và Bản đồ 61: 33-40.

[25] Luong, N. V., Duc Anh, N., Tu, T. T., Nandy, S., Lap, Q. K. (2025): Assessing The Significance of Trees Outside Forests in Northeastern Vietnam: Integration of Field Survey and Remote Sensing Data. – Applied Ecology & Environmental Research 23(1): 41-60. DOI: http://dx.doi.org/10.15666/aeer/2301_041060.

[26] Lưu Hồng Trường, Huỳnh Quang Thiện, Trần Văn Bằng, Nguyễn Lê Xuân Bách, Nguyễn Thành Trung, Đoàn Mạnh Tuấn (2024): Báo cáo hiện trạng đa dạng sinh học Vườn quốc gia U Minh Thượng (gốc)/Report on the current status of biodiversity in U Minh Thuong National Park (translated by N.V. Luong). – Kiên Giang, năm 2024.

[27] Manna, S., Nandy, S., Chanda, A., Akhand, A., Hazra, S., Dadhwal, V. K. (2014): Estimating aboveground biomass in *Avicennia marina* plantation in Indian Sundarbans using high-resolution satellite data. – Journal of Applied Remote Sensing 8(1): 083638. https://doi.org/10.1117/1.JRS.8.083638.

[28] Mougin, E., Proisy, C., Marty, G., Fromard, F., Puig, H., Betoulle, J. L., Rudant, J. P. (1999): Multifrequency and multipolarization radar backscattering from mangrove forests. – IEEE Transactions on Geoscience and Remote Sensing 37(1): 94-102. DOI: 10.1109/36.739128.

[29] Nandy, S., Ghosh, S., Kushwaha, S. P. S., Senthil Kumar, A. (2019): Remote sensing-based forest biomass assessment in northwest Himalayan landscape. – In: Navalgund, R., Kumar, A., Nandy, S. (eds.) Remote Sensing of Northwest Himalayan Ecosystems. Springer, Singapore, pp. 285-311. https://doi.org/10.1007/978-981-13-2128-3_13.

[30] Omar, H., Misman, M., Kassim, A. (2017): Synergetic of PALSAR-2 and Sentinel-1A SAR polarimetry for retrieving aboveground biomass in dipterocarp forest of Malaysia. – Applied Sciences 7(7): 675. https://doi.org/10.3390/app7070675.

[31] Omar, H., Misman, M. A., Yaakub, S. Y. (2020, July): Vegetation indices for identifying Melaleuca Forest from multispectral satellite sensors. – In: IOP Conference

Series: Earth and Environmental Science 540(1): 012009. IOP Publishing. DOI: 10.1088/1755-1315/540/1/012009.

[32] Opelele, O. M., Yu, Y., Fan, W., Chen, C., Kachaka, S. K. (2021): Biomass estimation based on Multilinear regression and machine learning algorithms in the Mayombe tropical forest, in the Democratic Republic of Congo. – Appl. Ecol. Environ. Res 19(1): 359-377. DOI: http://dx.doi.org/10.15666/aeer/1901_359377.

[33] Raihan, A., Begum, R. A., Said, M. N. M. (2021): A meta-analysis of the economic value of forest carbon stock. – Geografia 17(4): 321-338. https://doi.org/10.17576/geo-2021-1704-22.

[34] Rouse, J. W., Haas, R. H., Schell, J. A., Deering, D. W. (1974): Monitoring Vegetation Systems in The Great Plains with ERTS. – Remote Sensing Center, Texas.

[35] RSIS (2015): U Minh Thuong National Park. – Ramsar Sites Information Service: https://rsis.ramsar.org/ris/2228.

[36] Singh, A., Kushwaha, S. K. P., Nandy, S., Padalia, H., Ghosh, S., Srivastava, A., Kumari, N. (2023): Aboveground Forest Biomass Estimation by the Integration of TLS and ALOS PALSAR Data Using Machine Learning. – Remote Sensing 15(4): 1143. https://doi.org/10.3390/rs15041143.

[37] Stratoulias, D., Nuthammachot, N., Suepa, T., Phoungthong, K. (2022): Assessing the spectral information of Sentinel-1 and Sentinel-2 Satellites for above-ground biomass retrieval of a tropical forest. – ISPRS International Journal of Geo-Information 11(3): 199. https://doi.org/10.3390/ijgi11030199.

[38] Tran, D. B., Dargusch, P., Moss, P., Hoang, T. V. (2013): An assessment of potential responses of Melaleuca genus to global climate change. – Mitigation and Adaptation Strategies for Global Change 18(6): 851-867. https://doi.org/10.1007/s11027-012-9394-2.

[39] Tsitsi, B. (2016): Remote sensing of aboveground forest biomass: A review. – Tropical Ecology 57(2): 125-132.

[40] Tuong, T. C., Tani, H., Wang, X. F., Pham, V. M. (2019): Estimating aboveground biomass of bamboo and mixed bamboo forest in Thua Thien-Hue province, Vietnam using PALSAR-2 and Landsat OLI data. – The International Archives of Photogrammetry, Remote Sensing and Spatial Information Sciences 42: 11-19. https://doi.org/10.5194/isprs-archives-XLII-4-W20-11-2019.

[41] Vafaei, S., Soosani, J., Adeli, K., Fadaei, H., Naghavi, H., Pham, T. D., Tien Bui, D. (2018): Improving accuracy estimation of Forest Aboveground Biomass based on incorporation of ALOS-2 PALSAR-2 and Sentinel-2A imagery and machine learning: A case study of the Hyrcanian forest area (Iran). – Remote Sensing 10(2): 172. https://doi.org/10.3390/rs10020172.

[42] Williams, A. B. (1984): Shrimps, lobsters, and crabs of the Atlantic coast of the eastern United States, Maine to Florida. – Washington, DC: Smithsonian Institution Press. https://doi.org/10.2307/1352125.

[43] Xiang, L., Yao, S., Hua, W., Zhang, H., Jiang, J., Chen, Q., Chen, C., Chen, P., Sang, K. (2025): Fuzzy-Set Qualitative Comparative Analysis of Wetland Gross Ecosystem Product: The Case of Huaduhu Wetland Park in China. – Applied Ecology and Environmental Research 23(4): 8225-8249. DOI: http://dx.doi.org/10.15666/aeer/2304_82258249.

[44] Xiao, J., Chevallier, F., Gomez, C., Guanter, L., Hicke, J. A., Huete, A. R., Ichii, K., Ni, W., Pang, Y., Rahman, A. F., Sun, G., Yuan, W., Zhang, L., Zhang, X. (2019): Remote sensing of the terrestrial carbon cycle: A review of advances over 50 years. – Remote Sensing of Environment 233: 111383. https://doi.org/10.1016/j.rse.2019.111383.

[45] Zhao, P., Lu, D., Wang, G., Wu, C., Huang, Y., Yu, S. (2016): Examining spectral reflectance saturation in Landsat imagery and corresponding solutions to improve forest aboveground biomass estimation. – Remote Sensing 8(6): 469. https://doi.org/10.3390/rs8060469.

[46] Zhu, Y., Feng, Z., Lu, J., Liu, J. (2020): Estimation of Forest Biomass in Beijing (China) Using Multisource Remote Sensing and Forest Inventory Data. – Forests 11(2): 163. https://doi.org/10.3390/f11020163.


http://www.aloki.hu ● ISSN 1589 1623 (Print) ● ISSN 1785 0037 (Online)
DOI: http://dx.doi.org/10.15666/aeer/2401_14531466